Tribology and Materials
Vol. x, No. x, 202x, pp. xx-xx

ISSN 2812-9717
https://doi.org/10.46793/tribomat.2026.009

The effect of reinforcement on the properties of FeNiCuAl medium-entropy alloy

Dyna AYUNITA [1], Suprianto [1,*], Muhammad DALIL [2], Tulus Burhanuddin SITORUS [1], Bakhrul ILMI [1], Hazwan Chaitami HARAHAP [1], Khalbi AYUB [1]

[1] Faculty of Engineering, Universitas Sumatera Utara, Medan, Indonesia
[2] Faculty of Engineering, Universitas Riau, Pekanbaru, Indonesia
*Corresponding author: suprianto@usu.ac.id

Keywords

composite
dispersion strengthening
medium-entropy alloy
TiC
Y_2O_3

History

Received: 05-12-2025
Revised: 18-03-2026
Accepted: 06-04-2026

Abstract

Medium-entropy alloys (MEAs) are promising candidates in the engineering field due to their high strength. Their characteristics are strongly correlated with strengthening mechanisms. A combination of both solid solution and dispersion of ceramic particles influences strength improvement. These strengthening mechanisms are widely used in different alloys. However, the effectiveness of hybrid reinforcement particles in FeNiCuAl MEAs remains challenging. This study aims to investigate the effects of Y_2O_3 and TiC particles on the mechanical and tribological properties of FeNiCuAl-Y_2O_3/TiC synthesised by powder metallurgy. The microstructure, fracture and wear morphologies of the matrix and composites were analysed using a scanning electron microscope (SEM) and energy-dispersive spectroscopy (EDS). The mechanical properties, such as Vickers hardness and compressive strength, were measured. Furthermore, tribological properties were determined via dry sliding testing. The results show that the presence of reinforcement particles in the FeNiCuAl matrix increases hardness and reduces the wear rate. The addition of 1.5 wt. % TiC significantly improves wear resistance. On the other hand, the presence of Al indicates higher compressive and yield stresses of more than 350 MPa, obtained by adding 1.0 at. % Al into the FeCuNi alloy. In this study, the addition of reinforcement enhances hardness and wear resistance while reducing the ductility of the FeNiCuAl MEA.

1. Introduction

Medium-entropy alloys (MEAs) are widely used in engineering, such as functional, structural materials and mechanical components operated at high temperatures. This is due to their good mechanical and thermal properties. The combination of these elements makes them a promising candidate for mechanical components. Various methods can be used to synthesise MEAs, like casting and powder metallurgy. The powder metallurgy method can be used to produce CuNiCr, CuCrFeNi and Cu-B_4C materials [1-3]. This method can also be used to synthesise elements and materials containing large differences in melting temperatures, such as W, Cu, Ni, Fe, Al and ceramics. A different melting temperature of constituent elements of the AlCrFeTiCu and AlCrFeTiNi alloys [4] and CrFeNi-Y_2O_3 composites [5] were successfully synthesised by powder metallurgy. Furthermore, the characteristics of the MEAs are strongly influenced by the constituent elements with their origin characteristics.

The Fe promoted densification, plasticity and microstructural refinement in FeCu [6] and AlCoCrFexNi alloys [7]. The Cu has a good conductivity. It was reported that CuNiCoSi alloys show better electrical and wear resistance than CuNi2Si [8]. The addition of Mo refractory element also improves the hardness and wear resistance of the AlCoCrFexMo0.5Ni alloy [9]. Furthermore, the

CuCrFeNi MEA shows a better yield strength with Cu10, and its strengthening mechanism is also influenced by Cr carbide formation [2]. The combination of transition elements has the potential to be used as MEAs, in which a high hardness is obtained in the CoCrNi alloy [10]. The wear rate of the CuMnNi alloy decreases with the addition of the Sn [11]. The addition of Al to TiZrHf MEA led to phase evolution and solid-solution strengthening [12]. This element improves yield strength through crystallite change of the CrCoNi MEA [13]. Furthermore, the strengthening mechanism can also be achieved by using dispersed particles.

The TiC particles improve hardness and wear resistance through dispersion strengthening [14]. The combination of AlFeCrCo MEA and TiC resulted in an increase in wear resistance with the increase in particle amount [15]. The TiC particles reduce the wear of the Co37Cr28Ni31Al2Ti2 MEA with an abrasive model [16] and improve the hardness of the CoCrNi composites. However, they decrease ductility and brittle fracture [17]. In addition to TiC particles, dispersion strengthening was achieved using oxide particles. The addition of Y_2O_3 into Co-Al-W causes the microstructure evolution, in which finer grains and high hardness are obtained [18]. Wear resistance of AZ91 magnesium alloy improved by the increase of Y_2O_3 amount in the Al-Si coating [19]. These particles also significantly contributed to the strengthening of the FeCoNiCr alloy [20]. In the FeMnNiCr MEA, the addition of the Y_2O_3 enhances the oxidation resistance of this alloy [21]. The presence of a few TiC and Y_2O_3 particles has a positive effect on the characteristics of the alloys, particularly hardness and wear resistance, as reported in numerous studies.

The addition of 1 at. % Al with a low melting point is expected to contribute to filling the voids between particles during high-temperature sintering (1050 °C), thereby facilitating bonding between particles. Furthermore, the combination of TiC and Y_2O_3 has tremendous potential as a reinforcing particle in FeNiCuAl MEA, but studies on its strengthening mechanism are still limited. This study aims to investigate the influence of reinforcement particles on the microstructure, density, hardness and tribological behaviour of MEA, with special emphasis on the mechanisms of dispersion strengthening. The MEAs with different reinforcement compositions were synthesised via powder metallurgy.

2. Materials and methods

2.1 Materials

High-purity elemental powders consist of Cu (> 99.9 %), Ni (> 99.96 %), Fe (> 98.5 %) and Al (> 99.8 %) with particle sizes of 30 – 40 µm. In this study, Y_2O_3 and TiC with particle sizes of 44 µm and 1.4 µm, respectively, have been used as reinforcement materials. These materials were used as starting materials to synthesise the FeNiCuAl MEA-based composites, as shown in Table 1.

The first step involves weighing the matrix, consisting of FeNiCuAl with the compositions shown in Table 1 (in at. %). In the second step, the prepared matrix is mixed with the reinforcement in a ratio of 98 wt. % to 2 wt. % (totalling 100 wt. %) using a V-mixer for 120 minutes at 120 rpm. This mixing model is also equipped with a hard steel ball 8.0 mm in diameter and a ball-to-powder weight ratio of 10 : 1. A Mixing process under dry conditions, without a process control agent, was conducted to obtain a homogeneous distribution of constituent elements.

The first densification stages were achieved by cold compaction using a uniaxial hydraulic press with a capacity of 30 tons, operated at a constant pressure of 310 MPa for 15 minutes at room temperature. The compaction process uses a mould and a pin made from hard steel, with an inside diameter of 9.53 mm and a height of 25.53 mm. Furthermore, the compacted materials were sintered at 1050 °C for 60 minutes using conventional sintering to achieve final densification of the bulk material.

Table 1. Designation and composition of the FeNiCuAl MEA reinforced by Y_2O_3 and TiC particles

Designation	Material	Matrix, at. %				Reinforcement, wt. %	
		Fe	Ni	Cu	Al	Y_2O_3	TiC
MEA-Al	FeNiCuAl	35	33	31	1	–	–
MEA-2YO	FeNiCuAl2Y_2O_3	35	33	31	1	2	–
MEA-TiC	FeNiCuAlY_2O_3TiC	35	33	31	1	0.5	1
MEA-1.5TiC	FeNiCuAl$Y_2O_3$1.5TiC	35	33	31	1	0.5	1.5

2.2 Microstructural analysis

The microstructural analysis focuses on characterising the porosity, oxide particles and elemental distribution of the sintered MEA-Al alloy and the MEA-1.5TiC composite. Furthermore, fracture morphology was analysed by SEM to investigate the fracture mechanisms of the MEA-Al alloy and the MEA-1.5TiC composite. The details of the wear track of the brittle sample (MEA-1.5TiC) were investigated using SEM and EDS. In this study, the SEM analysis was conducted by using a Thermo Fisher Axia ChemiSEM SEM. Furthermore, the amounts of each constituent element in the selected area and the mapping area were obtained by EDS.

2.3 Physical, mechanical and tribological characterisation

The sintered density is measured using Archimedes' principle (ASTM B962). Relative density is calculated relative to the theoretical density of each sintered material. Further, the theoretical densities were 8.63, 8.36, 8.37 and 8.36 g/cm^3 for MEA-Al, MEA-2YO, MEA-TiC and MEA-1.5TiC, respectively. The dimensions of the compression test specimen were according to the ASTM B925. The testing was conducted by a universal testing machine model TN20MD with a 30 kN capacity and a 5 mm/min loading rate at room temperature. The Vickers hardness testing was conducted using a Shimadzu hardness tester with a load of 1 kgf and a dwell time of 10 seconds. The tribological test was in accordance with the ASTM G99, under dry sliding conditions, at a controlled load of 10 N (0.127 MPa), a sliding speed of 6.28 m/s and a sliding distance of 7536 m with a sliding time of 20 minutes at room temperature, using a cylindrical pin with a diameter of 10 mm and a height of 10 mm. The disc (counter-body), with a diameter of 170 mm and a thickness of 9 mm, was made of AISI 52100 steel with a hardness above 800 HV. To ensure data reproducibility and reliability, each test was conducted on three specimens (triplicate measurements) for each material.

3. Results and discussion

3.1 Microstructure

The microstructural analysis was conducted and focused on two samples that showed contrasting characterisation results. The MEA-Al is the sample with the lowest performance, while MEA-1.5TiC is the sample with the highest performance in terms of hardness, compressive strength and wear resistance. Figure 1 and Table 2 show SEM and EDS analyses of selected areas of the MEA-Al alloy and the MEA-1.5TiC composite. The microstructure consists of a solid solution phase, associated with a FeNiCu-rich area of light grey colour. Small pores containing oxide particles are associated with a dark area dispersed within the solid solution matrix. Reactive Al elements are believed to form an oxide during high-temperature sintering. On the other hand, the MEA-1.5TiC composite (Fig. 1b)

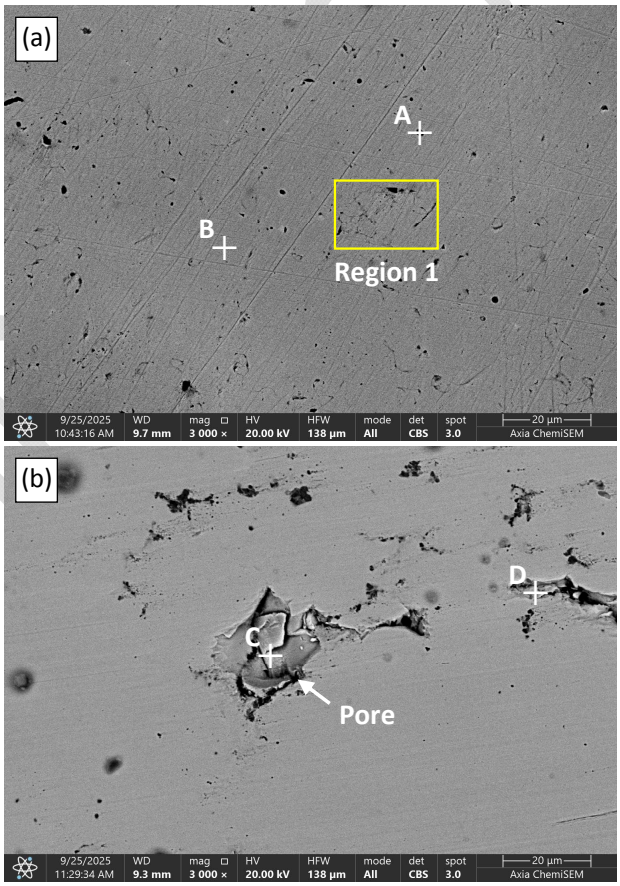

Figure 1. SEM micrographs with positions of the EDS analysis of: (a) MEA-Al alloy, and (b) MEA-1.5TiC composite

Table 2. EDS analysis results of the MEA-Al alloy and MEA-1.5TiC composite in selected areas of Figure 1

Area	Element, at. %							
	Fe	Ni	Cu	O	Al	C	Ti	Y
A	46.2	12.5	9.7	26.9	4.7	–	–	–
B	38.9	35.2	23.0	2.5	0.4	–	–	–
Region 1	36.9	35.6	24.9	2.2	0.4	–	–	–
C	19.9	33.3	18.9	12.4	0.5	14.2	0.8	–
D	9.5	41.6	24.2	5.0	0.3	19.3	0.1	–

shows more pores near the Ti- and C-rich regions. This result might be due to a thermal expansion mismatch between the ceramic particles and the metallic matrix. The formation of oxides and porosities around hard particles also occurred in the WCCo-based alloys [22].

Porosities of less than 2.53 and 4.73 µm in size formed in the MEA-Al alloy and the MEA-1.5TiC composite, respectively. The EDS analysis shows a significant difference in the elemental composition of selected areas within the MEA-Al alloy (Fig. 1a) and the MEA-1.5TiC composite (Fig. 1b). The areas A, B and Region 1 are dominated by Fe (36.9 to 46.2 at. %), followed by Ni and Cu elements, Al (0.4 to 4.7 at. %) and O (2.2 to 26.9 at. %). These findings confirmed that the Fe-Cu-Ni solid solution areas and the Al correspond to the alloy design shown in Table 1.

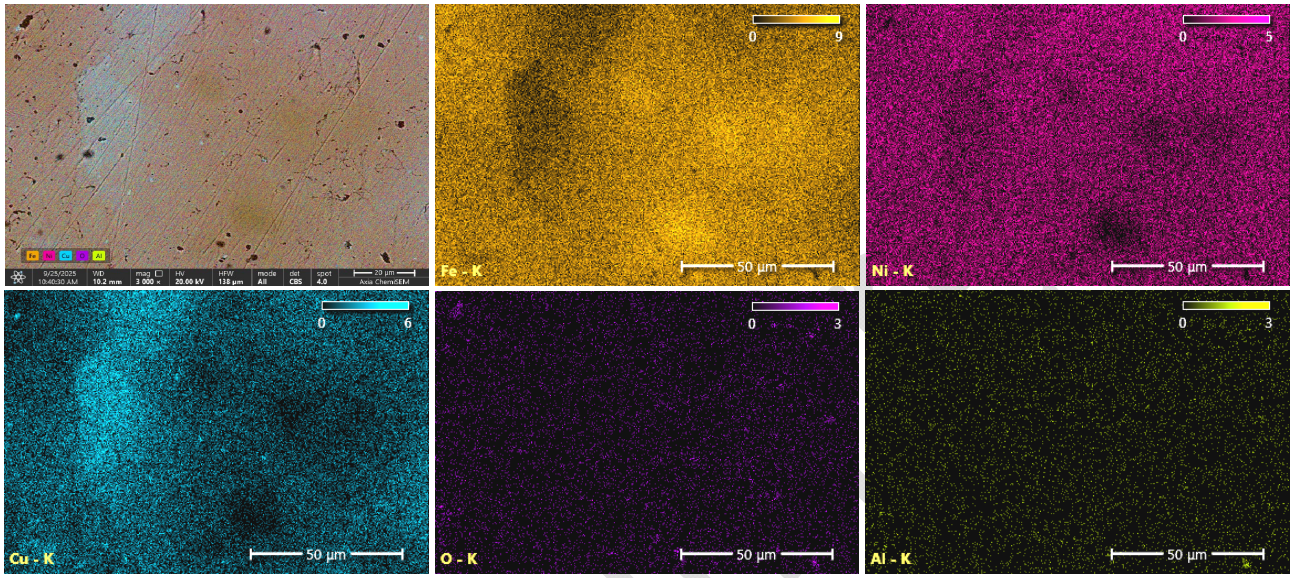

Figure 2. SEM micrograph and corresponding EDS elemental mapping of the MEA-Al alloy

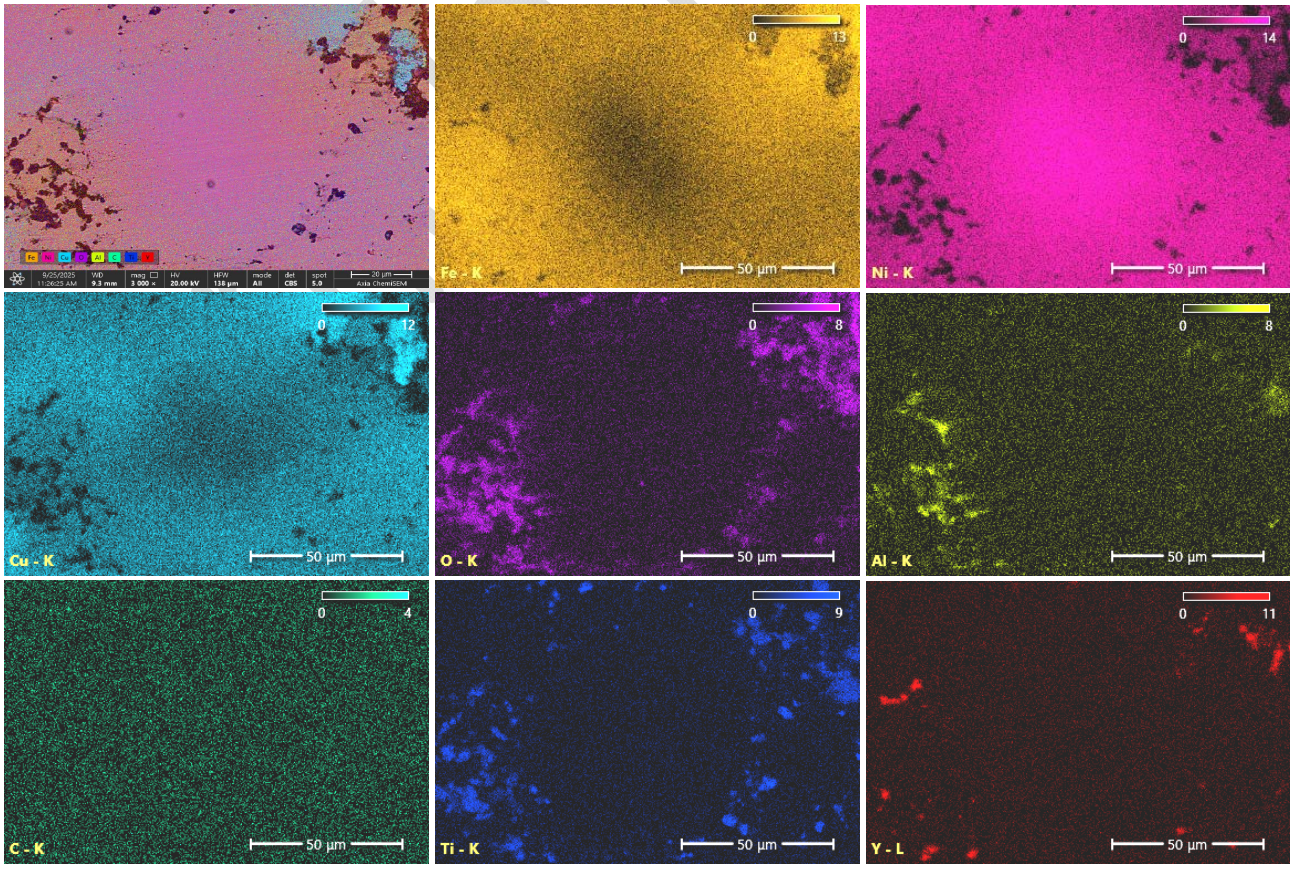

Figure 3. SEM micrograph and corresponding EDS elemental mapping of the MEA-1.5TiC composite

Meanwhile, the EDS analysis of the MEA-1.5TiC composite (areas C and D) revealed the presence of Ti (0.1 to 0.8 at. %) and C (14.2 to 19.3 at. %). This result confirms that the TiC particles were dispersed within the matrix. A similar phenomenon was reported in FeCoNiCuAl reinforced with TiC particles [23]. However, a nonhomogeneous distribution of TiC particles is dispersed within the solid solution matrix. These particles have difficulty dissolving into the FeNiCuAl matrix, but the ceramic particles can act as nucleation sites and dispersion-strengthening agents. In areas C and D, Ni and Cu are predominantly detected, confirming that the small ceramic particle acted as a nucleation site for other elements. The TiC acts as a nucleation site, further reducing the grain size, as noticed for the AlZnMgCu alloy [24]. Point C shows a high O concentration (12.4 at. %), which might correlate with the fact that the area is located close to the interface between the particle and the FeNiCu-rich phase, in which pores (dark area) formed with a higher O concentration. The formation of some pores within the interface of Cu-alloy and TiC is due to the presence of air trapped in the microstructure during powder processing [25].

The EDS elemental mapping of the MEA-Al alloy (Fig. 2) mainly revealed a uniform distribution of Fe, Ni, Cu, O and Al elements throughout the microstructure. However, Cu segregation in the microstructure of MEA-Al alloy was noticed. The Cu segregation is a complex mechanism, and mixing, sintering conditions and particle sizes may influence this phenomenon. The segregation of a small amount of each Ti, Y, Al and O was noticed in the microstructure of MEA-1.5TiC composite (Fig. 3). It is clearly visible that partially clustered Ti and O were dispersed in similar areas within the microstructure. This fact may correlate with the high-temperature (1000 – 1200 °C) sintering process, which promotes typical Ti-oxide formation [26].

3.2 Physical properties

Figure 4 shows the density and relative density of the MEA reinforced with different particles. MEA-Al alloy demonstrated the highest density of 6.4 g/cm^3 and a relative density of 73.9 %. The low melting point of Al is believed to act as a melt filler within the FeNiCuAl microstructure, reducing porosity (see Fig. 1a).

The addition of TiC reinforcing particles reduced both density and relative density. The MEA-2YO composite and MEA-TiC composite exhibit densities of 5.7 and 5.8 g/cm^3 with relative densities of 68.2 and 68.8 %, respectively. The lowest values (5.6 g/cm^3 and 66.0 %) were obtained for the MEA-1.5TiC composite. A small amount of TiC in these alloys does not significantly reduce the density. However, the presence of the carbide particles might hinder atomic diffusion and promote porosity formation [27].

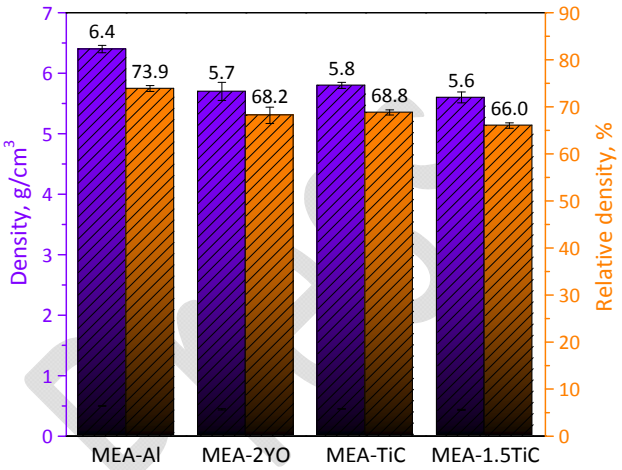

Figure 4. Density and relative density of the MEA alloy and composites

3.3 Mechanical properties

Figure 5 shows the hardness of four tested materials. The 231.8 HV1 and 299.2 HV1 were hardness values for the MEA-Al alloy and the MEA-2YO composite, respectively. This suggests that Y_2O_3 particles significantly enhance the strength. Furthermore, the addition of TiC continuously increases the hardness of MEA, with 364.9 HV1 for MEA-1.5TiC. The hardness increase is approximately 57 % with the addition of 1.5 wt. % TiC particles compared with the MEA-Al alloy. The presence of the TiC enhances the hardness of the MEA through the dispersion strengthening of hard particles within the FeNiCuAl solid solution matrix. The dispersion of TiC was also reported to improve the hardness of the Cu matrix composite [28].

Figure 6 shows the compressive stress of the MEA alloy and composites. The highest strain of more than 10 % and the compressive stress exceeding 461 MPa were noticed for the MEA-Al alloy. Because of its high plasticity, the MEA-Al alloy can undergo substantial plastic deformation before breaking, as demonstrated by this result. On the other hand, MEA reinforced with 2 wt. % Y_2O_3 and 1 wt.% TiC achieved peak stresses of approximately 214 MPa and 206 MPa, respectively, while exhibiting strains limited to 4 – 5 %. The MEA-1.5TiC composite exhibits the weakest

compressive stress, with a maximum stress of only 127 MPa and a strain capacity of 3 %.

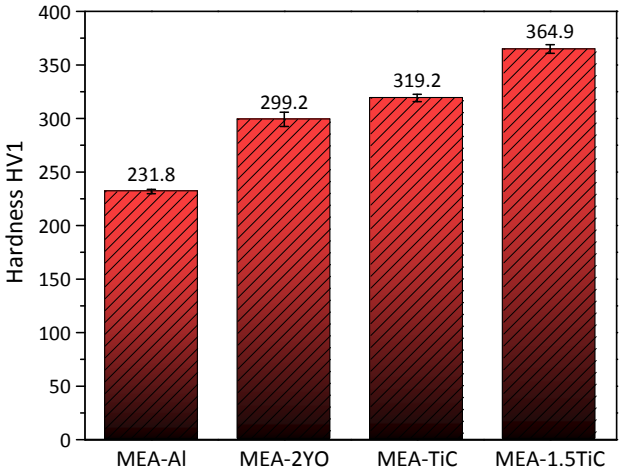

Figure 5. Hardness of the MEA alloy and composites

The combination of Y_2O_3 and TiC particles simultaneously compromises compressive stress and ductility. Pore formation, weak interface bonding and particle agglomeration are believed to influence the alloy's strength [29]. Even though the particles effectively hinder dislocation motion, stress concentrations could accelerate crack initiation or material failure [30], thereby diminishing plastic deformation capacity and reducing compressive strain. Not only TiC particles but also Y_2O_3 particles reduce the plastic strain of materials tested in this study (Fig. 6). Similarly, a lower strain was obtained for 15Cr-15Ni steel with the presence of Y_2O_3 particles in comparison with Y particles [31].

The analysis of fracture morphologies in Figures 7 and 8 focuses on comparing the characteristics of the most ductile (MEA-Al alloy) and the brittle (MEA-1.5TiC composite) sample, particularly highlighting the behaviour of the MEA-Al alloy and the influence of the dominant reinforcement particles. Figure 7 shows the fracture morphologies of the MEA-Al alloy. Dimples, tearing ridges and uniformly distributed small pores were noticed on the fracture surface. These shapes are typical for the microvoid coalescence process, which is prevalent in ductile materials that can undergo plastic deformation before breaking [32]. This behaviour is consistent with the compressive yield strength of MEA-Al alloy, which has a higher strain (Fig. 6) and is the sample with the best characterisation values.

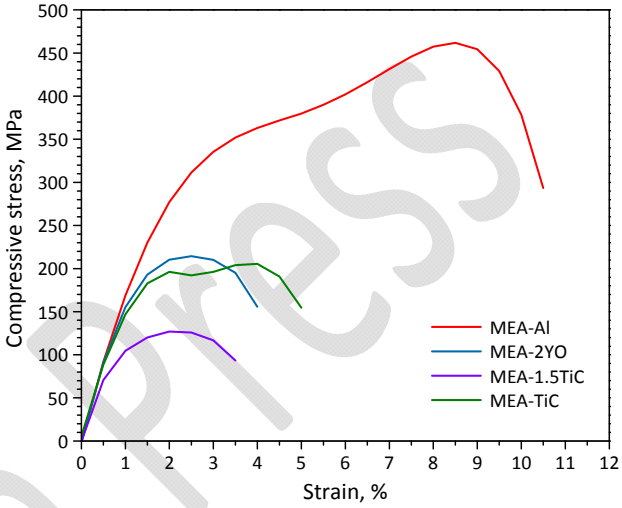

Figure 6. Compressive stress of the MEA alloy and composites

On the contrary, the fracture surface of the MEA-1.5TiC composite is dominated by granular rupture, shallow shear dimples, cracks and uneven dimple rupture, as shown in Figure 8. These morphologies indicated that plastic deformation is much more limited, and crack propagation occurs more rapidly. Finally, more brittle fractures were obtained. This result corresponds well with the compressive yield strength of the MEA-1.5TiC composite, as shown in Figure 6. It is believed that the higher TiC particle amount promoted agglomeration and porosity at the interface between the TiC particles and the FeNiCuAl matrix.

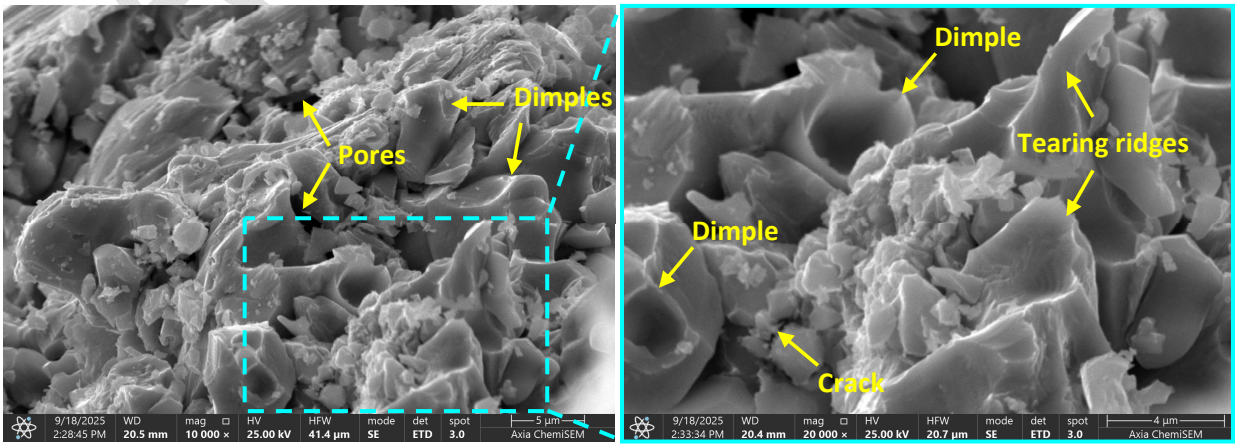

Figure 7. SEM micrographs of the fracture surface of MEA-Al alloy at different magnifications

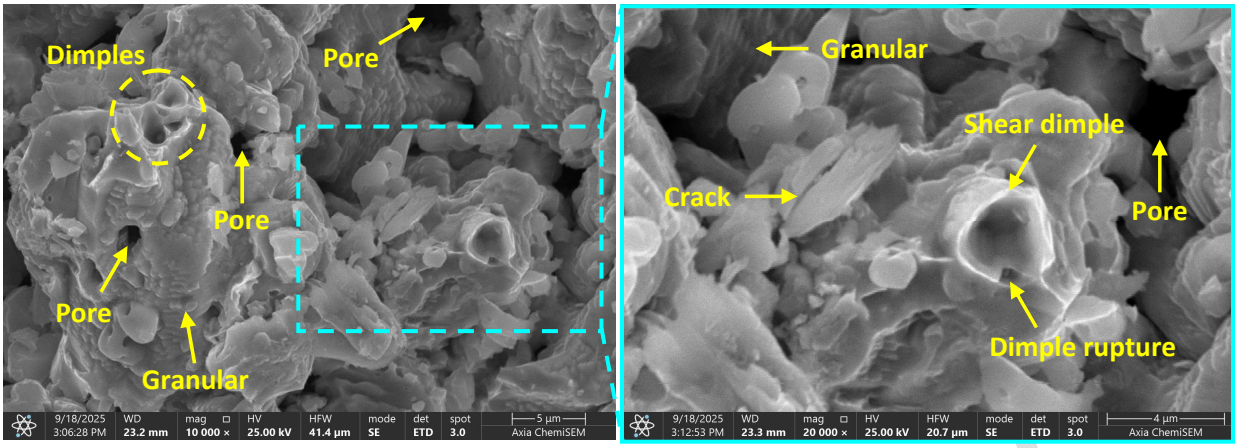

Figure 8. SEM micrographs of the fracture surface of MEA-1.5TiC composite at different magnifications

3.4 Tribological properties

Figure 9 shows the wear rate results of four tested materials. The wear rate decreases with the addition of ceramic particles into MEA. The MEA-Al alloy exhibited the highest wear rate of 1.58×10^{-3} mm^3/m, reflecting its relatively low wear resistance. Furthermore, the addition of 2 wt. % Y_2O_3 causes a slight decrease of the wear rate to 1.48×10^{-3} mm^3/m. The highest wear resistance showed the MEA-1.5TiC composite, with a wear rate of 1.13×10^{-3} mm^3/m. This result corresponds to the hardness values (Fig. 5). The TiC particles reduce the wear rate of the MEA significantly more than the addition of 2 wt. % Y_2O_3. This fact might be correlated with the particle acting as an obstacle to the plastic deformation and wear of the alloy [33].

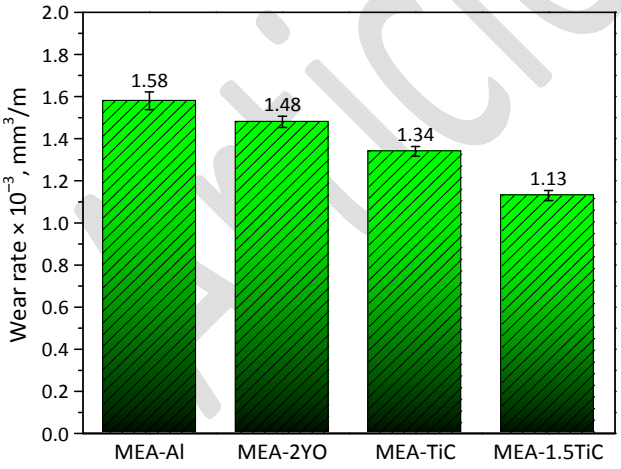

Figure 9. Wear rate of the MEA alloy and composites

Figure 10 illustrates the coefficient of friction of four tested materials. A coefficient of friction above 0.37 was noticed for the MEA-Al alloy, with a relatively constant value achieved after 3 minutes of sliding. The highest coefficient of friction corresponds to the high wear rate of the MEA-Al (Fig. 9). It is believed that the high coefficient of friction is correlated with the more particles pulled out from the surface during sliding. The coefficient of friction of the MEA-1.5TiC composite is also influenced by TiC and the matrix, with higher TiC content potentially increasing the coefficient of friction through the detachment of more TiC from the FeNiCuAl matrix. On the other hand, the MEA-2YO composite shows a lower coefficient of friction, with an average value of 0.24.

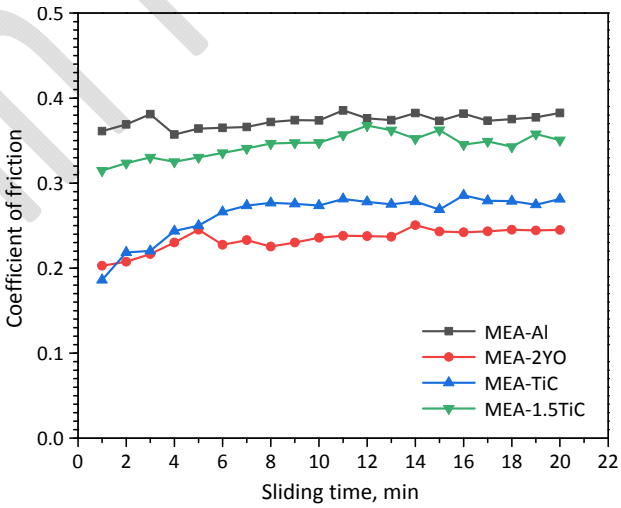

Figure 10. Coefficient of friction curve of the MEA alloy and composites

The worn surface morphology analysis was focused on the MEA-1.5TiC composite, which exhibits the lowest wear rate. The morphologies of the worn surface of the MEA-1.5TiC composite were analysed using SEM and EDS, as presented in Figure 11 and Table 3. The worn surface reveals localised plastic deformation and particle detachment, which promote abrasive and oxidative wear mechanisms. The EDS analysis at Point 1 shows that the surface contains Ni (30.1 at. %), Fe (22.7 at. %), O (14.2 at. %) and Ti (3.2 at. %). This composition indicates the presence of metal-oxide layers, suggesting that tribo-oxidation occurred during dry sliding and contributed to the development of protective

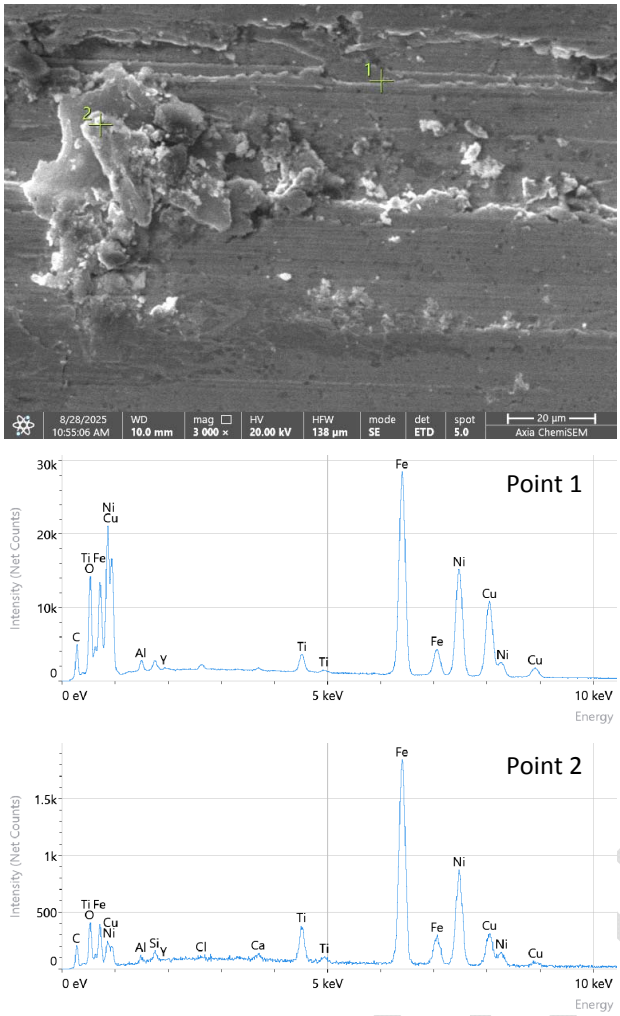

Figure 11. SEM image and EDS spectra of the selected area of the worn surface of the MEA-1.5TiC composite

Table 3. EDS analysis results of the MEA-1.5TiC composite in selected areas of Figure 11

Area	Element, at. %							
	Fe	Ni	Cu	Al	Y	O	Ti	C
Point 1	22.7	30.1	20.5	0.7	0.0	14.2	3.2	8.6
Point 2	34.8	23.4	8.9	0.8	0.1	11.4	3.8	15.1

surface films that enhance the wear resistance of the MEA-1.5TiC composite.

Meanwhile, Point 2 (Fig. 11) shows part of the peeled surface contact. The constituent element consists of Fe (34.8 at. %), Ni (23.4 at. %), O (11.4 at. %) and Ti (3.8 at. %). This result is consistent with the EDS spectra of the MEA-1.5TiC composite in point 2, which show the highest intensities for Fe and Ni. The higher Fe content in this area confirms that material removal occurs in Fe-rich areas, which subsequently leads to metal-oxide formation [34]. It is believed that the Fe in this area does not only come from the MEA-1.5TiC composite but can also be sourced from the counter-body material, which is AISI 52100 steel. The presence of Ti and C confirms the release of TiC particles within the tribological layer. The superior wear resistance of the MEA-1.5TiC composite is attributed to the synergistic effect of TiC particles and oxide film formation, as confirmed by SEM and EDS analysis.

Figure 12 shows a detail of the worn surface morphology of MEA-1.5TiC composite. The presence of grooves and spalled regions indicates that localised plastic deformation and layer detachment, resulting from cyclic sliding, occurred on the surface. Furthermore, shear stress generated surface delamination. At higher magnification, cracks and dispersed wear debris were noticed on the surface. This fine debris, which is formed during sliding, is less than 2 µm in size and irregularly shaped. Repeated high-stress contact and debris may be contributing to surface damage in the MEA reinforced with ceramic particles. For the magnesium alloy reinforced with SiC particles, it was suggested that the presence of fine debris within the contact area promoted surface cracks [35]. Based on SEM and EDS analysis of the worn surface, it is clear that the combination of abrasive wear, oxidative wear and spalling occurred as a wear mechanism in the MEA-1.5TiC composite.

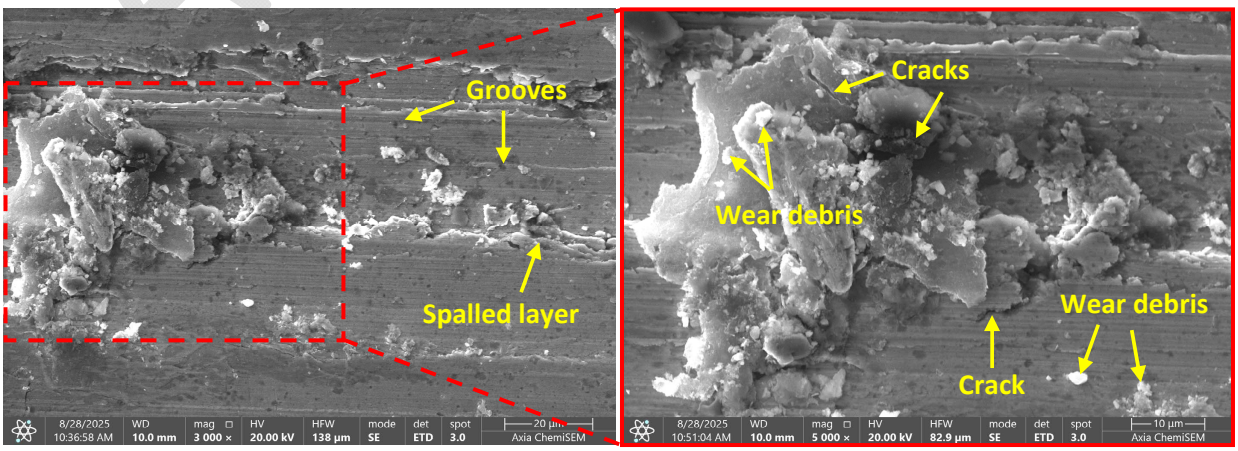

Figure 12. SEM micrographs of the worn surface of MEA-1.5TiC composite at different magnifications

4. Conclusion

Based on the results, several conclusions can be drawn regarding the characteristics of the FeNiCuAl MEA reinforced with Y_2O_3 and TiC particles. SEM images and EDS mapping show a homogeneous distribution of Al in the MEA-Al alloy. However, the addition of 1.5 wt. % TiC into FeNiCuAl shows some segregation of the TiC/Y_2O_3 particles, and a clustered Cu is also formed within the microstructure of the MEA-1.5TiC composite.

The highest hardness (364.9 HV1) corresponds to the lowest wear rate (1.13×10^{-3} mm^3/m), noticed for the MEA-1.5TiC composite. The SEM image of the worn surface of MEA-1.5TiC composite showed brittle fracture features, clustered (Ti, O)-rich elements in EDS point analysis, a protective tribo-oxide layer and cracks on the worn surface. This result confirms the role of TiC in the dispersion strengthening of MEA-1.5TiC composite. On the other hand, MEA-Al alloy shows the highest plastic deformation and yield stress of about 460 MPa, despite its low hardness. Furthermore, the SEM analysis of the fracture morphology revealed predominantly ductile dimples, indicating higher ductility.

The addition of TiC plays an important role in improving hardness and reducing the wear rate of the FeNiCuAl MEA. However, the TiC potentially decreases the ductility of the matrix MEA. These facts suggest that the correct amount of reinforcement particles and their distribution are important for balancing ductility, hardness, strength and wear resistance. Given its highest hardness and wear resistance, the MEA-1.5TiC composite can potentially be used in mechanical applications, such as gears and transmission components.

Acknowledgement

The authors would like to thank the Directorate of Research and Community Service (Indonesian: Direktorat Penelitian dan Pengabdian kepada Masyarakat/DPPM, Direktorat Jenderal Riset dan Pengembangan) of the Ministry of Higher Education, Science, and Technology of the Republic of Indonesia, for financial support of this current study under contract No. 111/UN5.4.10.K/PT.01.03/DPPM/2025.

References

[1] J.A. Guevara Carrió, M.A. Carvalhal, L.M. Ayabe, L.C.E. da Silva, R.V. Silva Junior, W.A. Monteiro, Microstructural and electrical investigation of Cu-Ni-Cr alloys obtained by powder metallurgy method, Materials Science Forum, Vol. 660-661, 2010, pp. 35-40, DOI: 10.4028/www.scientific.net/MSF.660-661.35

[2] P.B. Oboso, S. Oyama, J. Horioka, L.-F. Yi, T. Onda, S. Morito, Z.-C. Chen, Microstructure and mechanical properties of CuCrFeNi medium entropy alloys synthesized via mechanical alloying and spark plasma sintering, Journal of Alloys and Compounds, Vol. 1010, 2025, Paper 177700, DOI: 10.1016/j.jallcom.2024.177700

[3] B.K. Talluri, R. Narasimha Rao, M. Özcan, P. Syam Prasad, Evaluating mechanical and tribological performance of B_4C reinforced aluminum composites with predictive machine learning models, Results in Engineering, Vol. 27, 2025, Paper 106503, DOI: 10.1016/j.rineng.2025.106503

[4] N. Yurchenko, D. Shaysultanov, E. Povolyaeva, D. Moskovskikh, S. Zherebtsov, N. Stepanov, Structure and mechanical properties of low-density AlCrFeTiX (X = Co, Ni, Cu) high-entropy alloys produced by spark plasma sintering, Journal of Alloys and Compounds, Vol. 1007, 2024, Paper 176445, DOI: 10.1016/j.jallcom.2024.176445

[5] Z. Lu, S. Peng, H. Li, S. Gao, Improved oxidation resistance of ODS-CrFeNi medium entropy alloys by different Y_2O_3/Ti/Zr additions, Journal of Alloys and Compounds, Vol. 960, 2023, Paper 171017, DOI: 10.1016/j.jallcom.2023.171017

[6] S. Sutrisna, M.J. Purnomo, W. Wartono, A.B. Prasetiyo, M.I.S. Riadji, W.P. Mingwaro, Optimisation of microstructure and wear properties of porous Fe-Cu bearing materials, Tribology and Materials, DOI: 10.46793/tribomat.2026.004

[7] Q. Chen, K. Zhou, L. Jiang, Y. Lu, T. Li, Effects of Fe content on microstructures and properties of $AlCoCrFe_xNi$ high-entropy alloys, Arabian Journal for Science and Engineering, Vol. 40, No. 12, 2015, pp. 3657-3663, DOI: 10.1007/s13369-015-1784-9

[8] V. Karakurt, I. Esen, O. Zığındere, H. Ahlatci, Investigation of mechanical, electrical conductivity, wear and corrosion performances of traditional CuNi2Si and new high performance CuNiCoSi copper based alloys, Canadian Metallurgical Quarterly, Vol. 64, No. 3, 2025, pp. 1122-1148, DOI: 10.1080/00084433.2024.2425495

[9] C.-Y. Hsu, T.-S. Sheu, J.-W. Yeh, S.-K. Chen, Effect of iron content on wear behavior of AlCoCrFexMo0.5Ni high-entropy alloys, Wear, Vol. 268, No. 5-6, 2010, pp. 653-659, DOI: 10.1016/j.wear.2009.10.013

[10] F. Cao, P. Munroe, Z. Zhou, Z. Xie, Medium entropy alloy CoCrNi coatings: Enhancing hardness and damage-tolerance through a

nanotwinned structuring, Surface and Coatings Technology, Vol. 335, 2018, pp. 257-264, DOI: 10.1016/j.surfcoat.2017.12.021

[11] W. Bai, Y. Li, A. Zhang, B. Xin, J. Han, J. Meng, A novel $(CuMnNi)_{100-x}Sn_x$ medium entropy bronze alloys with excellent mechanical properties and wear resistance, Journal of Alloys and Compounds, Vol. 990, 2024, Paper 174471, DOI: 10.1016/j.jallcom.2024.174471

[12] P. Yuan, L. Wang, Y. Liu, X. Hui, Abnormal effect of Al on the phase stability and deformation mechanism of Ti-Zr-Hf-Al medium-entropy alloys, Metals, Vol. 14, No. 9, 2024, Paper 1035, DOI: 10.3390/met14091035

[13] Q. Hu, F. Liu, Q. Fan, H. Du, G. Liu, G. Wang, Z. Fan, X. Liu, Effect of Al on microstructure and mechanical properties of cast CrCoNi medium-entropy alloy, China Foundry, Vol. 15, No. 4, 2018, pp. 253-262, DOI: 10.1007/s41230-018-8031-4

[14] B. Wang, Y. Li, C. Guo, G. Huang, W. Li, Effects of TiC on the microstructure and mechanical properties of four Fe-based laser cladding coatings, Coatings, Vol. 14, No. 7, 2024, Paper 872, DOI: 10.3390/coatings14070872

[15] L. Ma, D. Zhao, Y. Wang, K. Wang, J. Huang, X. Jin, D. Kong, M. Wang, T. Yamaguchi, H. Wang, Optimized wear behaviors and related wear mechanisms of medium entropy alloy-based composite coatings, Journal of Materials Research and Technology, Vol. 29, 2024, pp. 12-27, DOI: 10.1016/j.jmrt.2024.01.108

[16] Y. Zhao, W. Ma, O. Tisov, Enhancing reciprocating wear resistance of Co37Cr28Ni31Al2Ti2 spark plasma sintered medium-entropy alloy via TiC addition, Materials, Vol. 18, No. 2, 2025, Paper 442, DOI: 10.3390/ma18020442

[17] Y. Cai, Y. Tong, Y. Hu, H. Huang, X. Zhang, M. Hua, S. Xu, Y. Mei, C. Ma, Z. Li, Wear-resistant TiC strengthening CoCrNi-based high-entropy alloy composite, Materials, Vol. 14, No. 16, 2021, Paper 4665, DOI: 10.3390/ma14164665

[18] C.-L. Chen, Suprianto, Influence of Ta and Y_2O_3 on synthesis, phase evolution and mechanical properties of Co-Al-W based alloys, Journal of Alloys and Compounds, Vol. 791, 2019, pp. 567-574, DOI: 10.1016/j.jallcom.2019.03.262

[19] X. Wan, C. Tian, Y. Li, J. Zhou, S. Qian, L. Su, L. Wang, Effect of Y_2O_3 addition on microstructure and properties of laser cladded Al-Si coatings on AZ91D magnesium alloy, Materials, Vol. 16, No. 1, 2023, Paper 338, DOI: 10.3390/ma16010338

[20] B. Jia, X. Liu, H. Wang, Y. Wu, Z. Lu, Microstructure and mechanical properties of FeCoNiCr high-entropy alloy strengthened by nano-Y_2O_3 dispersion, Science China Technological Sciences, Vol. 61, No. 2, 2018, pp. 179-183, DOI: 10.1007/s11431-017-9115-5

[21] Y.-Y. Wu, X.-J. Du, X.-Q. Jia, Z.-L. Xu, X.-T. Wu, Y.-Z. He, Y_2O_3-doped Fe-Mn-Ni-Cr medium entropy alloy with superior oxidation and spallation resistance fabricated by spark plasma sintering, JOM, Vol. 77, No. 6, 2025, pp. 4877-4892, DOI: 10.1007/s11837-025-07341-y

[22] S.V. Briakunov, A.S. Kurlov, Microstructure and phase composition of hard alloys produced from nanocrystalline powder mixture WC-6wt.%Co with C, Al and ZrC additives, Powder Metallurgy and Functional Coatings, Vol. 17, No. 1, 2023, pp. 49-62, DOI: 10.17073/1997-308X-2023-1-49-62

[23] T. Zhu, H. Wu, R. Zhou, N. Zhang, Y. Yin, L. Liang, Y. Liu, J. Li, Q. Shan, Q. Li, W. Huang, Microstructures and tribological properties of TiC reinforced FeCoNiCuAl high-entropy alloy at normal and elevated temperature, Metals, Vol. 10, No. 3, 2020, Paper 387, DOI: 10.3390/met10030387

[24] Q. Liao, J. Li, J. Liu, S. Lü, L. Chen, W. Guo, S. Wu, Effects of Al-Ti-C refiner and forming processes on the microstructure and properties of Al-Zn-Mg-Cu alloys, Materials, Vol. 15, No. 19, 2022, Paper 6960, DOI: 10.3390/ma15196960

[25] N.A. Abd, J.A. Yagoob, K.H. Razeg, The effect of micro and nano size TiC additions on some properties of copper fabricated by powder metallurgy, Journal of Nanostructures, Vol. 11, No. 3, 2021, pp. 588-600, DOI: 10.22052/JNS.2021.03.016

[26] X. Liu, Y. Chen, L. Li, H. Zhang, A. Huang, X. Fan, X. Zhao, J. Lu, Understanding the growth mechanisms of TiO_2/Al_2O_3 mixed scales formed on Al-depleted Ti_2AlC at 1000-1200 °C, Corrosion Science, Vol. 204, 2022, Paper 110393, DOI: 10.1016/j.corsci.2022.110393

[27] L. Huang, Y. Pan, J. Zhang, A. Liu, Y. Du, F. Luo, Densification, microstructure and mechanical performance of TiC/Fe composites by spark plasma sintering, Journal of Materials Research and Technology, Vol. 9, No. 3, 2020, pp. 6116-6124, DOI: 10.1016/j.jmrt.2020.04.014

[28] Z. Zhai, H. Dong, D. Li, Z. Wang, C. Sun, C. Chen, Effect of TiC particles on the properties of copper matrix composites, Inorganics, Vol. 12, No. 4, 2024, Paper 120, DOI: 10.3390/inorganics12040120

[29] K. Fazlur Rahman, B.M. Praveen, Interfacial characterization of graphene oxide and carbon nanotubes-strengthened aluminium matrix composites, International Journal of Scientific Research in Science and Technology, Vol. 11, No. 6, 2024, pp. 473-484, DOI: 10.32628/IJSRST24114305

[30] Y. Xia, X. Zhang, D. Zhao, X. Rong, C. He, N. Zhao, Breaking the strength-ductility trade-off for

metal matrix composites: A review of the role of nanoscale reinforcement dimension on the deformation and strengthening mechanisms, Review of Materials Research, Vol. 1, No. 1, 2025, Paper 100019, DOI: 10.1016/j.revmat.2025.100019

[31] R. Zhao, H. Jia, S. Cao, Z. Tong, Z. Zhou, Effect of the addition of Y and Y_2O_3 on microstructure and mechanical properties of 15Cr-15Ni ODS steel, Nuclear Materials and Energy, Vol. 31, 2022, Paper 101196, DOI: 10.1016/j.nme.2022.101196

[32] J. Zeng, J. Liu, Y. Jia, G. Zhao, Study on the deformation and fracture mechanisms of plastic metals considering void damage, Metals, Vol. 13, No. 9, 2023, Paper 1566, DOI: 10.3390/met13091566

[33] A. Vencl, Tribological behavior of ferrous-based APS coatings under dry sliding conditions, Journal of Thermal Spray Technology, Vol. 24, No. 4, 2015, pp. 671-682, DOI: 10.1007/s11666-014-0202-2

[34] H. Lee, J. An, S. Jeong, K. Nam, Advanced spectroscopic evidence for the sequestration of heavy metals via repetitive in situ synthesis of Fe oxide, Journal of Hazardous Materials, Vol. 486, 2025, Paper 137103, DOI: 10.1016/j.jhazmat.2025.137103

[35] M. Tayebi, A.R. Eivani, M. Kaseem, M. Mehdizade, H.R. Jafarian, Comparative study of wear behavior of magnesium matrix composite reinforced with silicon carbide particles and whiskers before and after extrusion, Journal of Magnesium and Alloys, Vol. 13, No. 10, 2025, pp. 5091-5114, DOI: 10.1016/j.jma.2025.08.019